



Porous heat-treated fungal biomass: preparation, characterization and application for removal of textile dyes from aqueous solutions

Bouthaina Ghariani¹ · Bilel Hadrich² · Ibtihel Louati¹ · Rim Mtibaà¹ · Dalel Daâssi³ · Susana Rodriguez-Couto^{4,5,6} · Moncef Nasri¹ · Tahar Mechichi⁷

Published online: 22 March 2019
© Springer Science+Business Media, LLC, part of Springer Nature 2019

Abstract

Fermentation process waste was used as an ideal alternative, with low cost and high efficiency, to the expensive methods of removing dyes from wastewater. In this study, granular particles of heat treated-lyophilized biomass of the fungi *Neonectria radiculicola* were tested to remove the three acid dyes Acid Orange 51 (AO 51), Reactive Red 75 (RR 75) and Direct Blue 86 (DB 86) from aqueous solutions and their adsorption was characterized in terms of adsorption isotherms and kinetics. Biosorption was investigated under different conditions of pH, contact time, temperature, adsorbent dosage and dye concentrations. The obtained results showed that optimum pH for dye adsorption was 2.0, the maximum uptake between 30 and 60 min of contact time and the equilibrium was reached within 60 min. The adsorption kinetics of the three dyes followed a pseudo-first-order rate model and Redlich–Peterson model fitted well the adsorption isotherms. The maximum adsorption capacities determined from the Redlich–Peterson equation were 120.6, 75.37 and 200.5 L g⁻¹ for AO 51, RR 75 and DB 86, respectively. FT-IR analysis indicates the involvement of various functional groups and SEM images showed morphological changes.

Keywords Bio-sorbent · Adsorption · Azo-dyes · Kinetics · Isotherms · Modeling

1 Introduction

Dye wastewater is one of the most important water pollution sources associated with several industries such as textile, paper, plastic, etc. The amount of dyes discharged from various processes in the environment cannot be exactly calculated. However, it is estimated that 100 tons/year of dyes are discharged into water streams with a use of more than 10,000 tones/year in the textile industry worldwide [1]. Dyes, even at low concentration (less than 1 ppm for some dyes), are becoming a relevant environmental issue by reducing water transparency and oxygen solubility and being often toxic and mutagenic for the aquatic flora and fauna [2]. However, the removal of these dyes, especially at low concentrations, from wastewater is a difficult challenge.

Recently, many biological and chemical techniques have been studied to remove dyes from wastewater such as aerobic and anaerobic microbial degradation, adsorption [3], membrane separation, coagulation, chemical oxidation and photo-catalytic degradation [4]. In aerobic and anaerobic systems, the biological activity of the microorganisms can be inhibited by the harsh environment (pH, salt concentration)

✉ Bouthaina Ghariani
bouthaina.ghar@live.fr

¹ Laboratory of Enzyme Engineering and Microbiology, National School of Engineers of Sfax, University of Sfax, BP 1173, 3038 Sfax, Tunisia

² Unité de Biotechnologie des Algues, Biological Engineering Department, National School of Engineers of Sfax, University of Sfax, BP 1173, 3038 Sfax, Tunisia

³ Department of Biology, Faculty of Sciences and Arts, Khulais, University of Jeddah, Jeddah, Saudi Arabia

⁴ Ceit, Paseo Manuel de Lardizábal 15, 20018 San Sebastián, Spain

⁵ Universidad de Navarra, Tecnun, Paseo Manuel de Lardizábal 13, 20018 San Sebastián, Spain

⁶ IKERBASQUE, Basque Foundation for Science, Maria Diaz de Haro 3, 48013 Bilbao, Spain

⁷ Laboratory of Biochemistry and Enzyme Engineering of Lipases, National School of Engineers of Sfax, University of Sfax, BP 1173, 3038 Sfax, Tunisia

while the physical and chemical treatments are usually technically or economically unfeasible [5, 6]. Also, the wide fluctuations in composition, pH and temperature of the dye-containing wastewater, make their treatment still more difficult to design and control [6]. The chemical treatments (Fenton reagent oxidation, ozonation, photochemical degradation and sodium hypochlorite addition) generate toxic compounds due the cleavage of the chromophoric groups [7]. In addition, anaerobic bioremediation can be affected by this phenomenon [8]. By contrast, adsorption is one of the most reliable and versatile physical methods for wastewater treatment characterized by high efficiency ease of operation and insensitivity to toxic pollutants. However, its effectiveness and economic sustainability is strictly related to the type of adsorbent [9]. For example, activated carbon is the most used adsorbent to remove pollutants from wastewater due to its high adsorption capacity towards different compounds [10]. However, regeneration of the used carbon is expensive (for example thermal regeneration costs about 1–2 US dollar/kg) [11].

In the last 20 years, research has been focused in developing low-cost and high effective adsorbents such as those based on natural materials (e.g. clay minerals and zeolites), bio-sorbents (microbial biomass: bacteria, yeasts, filamentous fungi and algae) and solid wastes from agriculture and industry (e.g. pine wood, corncob, bagasse, rice husk, chitosan, etc.). A number of metabolism-independent phenomena, like physical and chemical adsorptions, electrostatic interactions, ion exchange, complexation, chelation and macro precipitation, are involved in the process and mainly take place at cell wall level [12].

Since the 1980s, the use of live or dead biomass for adsorption studies has been successfully used, especially for the adsorption of heavy metals and some recalcitrant pollutants from effluents [13, 14]. Two main advantages are provided by dye adsorption on biomass: biomass is a cheap adsorbent, most of the time recovered as waste material [7] and the composition of the cell walls and the inactivation procedure (the disruption of cells after autoclaving) conduce to a wide diversity of the active sites and large specific surface.

To get a better understanding of the biosorption mechanism, both isotherms and kinetics of dye removal by fungal biomass in batch system were studied. In addition, the effect of experimental conditions on maximum dye removal efficiency was investigated. Thus, the aim of this study was to investigate not only the removal of different acid dyes under different experimental conditions by a new bio-sorbent prepared from the fermentation process waste of the fungi *Neonectria radicularis*, but also to characterize the biosorption equilibrium and kinetics towards the studied dyes.

2 Experimental

2.1 Preparation of the dye solutions

Three different dyes were investigated in this study, namely Acid Orange 51 (AO 51), Reactive Red 75 (RR 75) and Direct Blue 86 (DB 86). Stock solutions of each dye were prepared by dissolving 50 mg of dye in 50 mL of distilled water. Different concentrations ranged between 25 and 1000 mg L⁻¹ of each dye were obtained by appropriate dilution of the stock solutions. The maximum absorbance (λ_{max}) of each dye was determined by UV–Visible spectrophotometry (JENWAY 7315 Spectrophotometer). In Table 1 the chemical structure and some characteristics of the above mentioned dyes are shown.

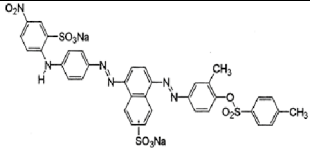
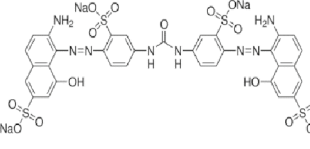
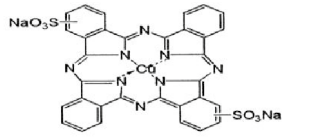
2.2 Fungal strain, culture conditions and bio-sorbent material preparation

The fungal strain used in this study was isolated from decaying acacia wood in the northwest of Tunisia and identified as *Neonectria radicularis* [15]. The strain was maintained on Petri plates containing 2% malt extract agar (MEA) at 4 °C and sub-cultured every month. Mycelia suspension of the fungal strain were obtained by inoculating four plugs (1 cm²), cut from the growing zone of a 5-day-old fungus grown on Petri plates, into 1000 mL cotton plugged Erlenmeyer flasks containing 250 mL of malt extract medium (18 g L⁻¹). After one week of incubation, fungal biomass was harvested and thoroughly washed with distilled water to remove the culture medium. The resulting biomass was autoclaved at 121 °C for 45 min in order to kill the fungal cells and finally lyophilized, powdered and sieved to obtain very fine particles. The average size of these particles, which will serve as the biosorbent, was evaluated to be in the range of 250 µm.

2.3 Dye bio-sorption assays

For dyes bio-sorption, a constant mass of the bio-sorbent was mixed with different concentrations of each dye in 50 mL Erlenmeyer flasks containing 10 mL of dye solutions. The flasks were incubated at 150 rpm and room temperature (30 °C). In order to determine the optimum biosorption conditions, experiments were performed by varying the following experimental parameters: pH values (2–12), bio-sorbent quantity (0.25–1.5 g), initial dye concentrations (25–1000 mg L⁻¹) and contact time (0–120 min). The initial pH of the experiment was adjusted by adding 0.1 M HCl or 0.1 M NaOH. At the end of the contact time, the bio-sorbent was separated by centrifugation, followed by the analysis of the supernatant for residual dye concentration.

Table 1 Physicochemical characteristic of Acid Orange 51, Reactive Red 75 and Direct Blue 86

Dye	Class	λ_{\max} (nm)	Chemical structure
AO 51	Azoic	452	
RR 75	Azoic	522	
DB 86	Phthalocyanine	606	

All experiments were conducted in duplicate. Dyes removal efficiency was determined by Eq. (1):

$$\% \text{ dye removal} = \frac{(C_0 - C_f) * 100}{C_0} \quad (1)$$

where C_0 and C_f are the initial and equilibrium dye concentration (mg L^{-1}), respectively.

The amount of dye adsorbed onto a unit weight of the adsorbent q_e (mg g^{-1}) was calculated using the mass balance equation given by Eq. (2):

$$q_e = \frac{V * (C_0 - C_f)}{M} \quad (2)$$

where: q_e is the quantity of adsorbed dye per unit mass of bio-sorbent (mg g^{-1}), V is the solution volume (L), M is the bio-sorbent mass (g).

2.4 Modeling of bio-sorption kinetics

Among several kinetics models, pseudo-first order, pseudo-second order, intra-particle diffusion and Elovich models were tested to describe the experimental data. Kinetics studies for adsorption of dyes were conducted at 50 mL Erlenmeyers with 10 mL of initial dyes concentration of 50 and

100 mg L^{-1} , containing 1 g L^{-1} of bio-sorbent at temperature of 30 °C and 150 rpm for 60 min.

2.4.1 The pseudo-first-order model

The pseudo-first-order model equation is expressed as follows [16]:

$$\frac{dq(t)}{dt} = k_1 \cdot (q_e - q(t)) \quad (3)$$

After integrating by applying the boundary conditions, the following equation can be obtained:

$$q(t) = q_e \cdot (1 - e^{-k_1 t}) \quad (4)$$

where q_e and q (mg g^{-1}) are the amounts of dyes adsorbed by the biomass at equilibrium and at any time t respectively, and k_1 (min^{-1}) is the pseudo first order rate constant.

2.4.2 The pseudo-second-order model

The pseudo-second-order model proposed by [17] assumes that the adsorption process follows second-order chemisorptions. It can be expressed as:

$$\frac{dq(t)}{dt} = k_2 \cdot (q_e - q(t))^2 \quad (5)$$

After integrating for the same boundary conditions, the Eq. (5) becomes:

$$q(t) = \frac{k_2 \cdot q_e^2 \cdot t}{1 + k_2 \cdot q_e \cdot t} \quad (6)$$

where k_2 ($\text{g mg}^{-1} \text{min}$) is the pseudo-second order rate constant of the adsorption.

2.4.3 The intra-particle diffusion model

To elucidate the dye diffusion mechanism into biomass, the mathematical formula for the intra-particle diffusion model, as indicated in Eq. (7), was used [18]:

$$q(t) = k_p \cdot t^{1/2} + c \quad (7)$$

where: c is the intercept (mg g^{-1}) and k_p is the intra-particle diffusion rate constant ($\text{mg g}^{-1} \text{min}^{-1/2}$).

2.4.4 The Elovich model

The Elovich model is one of the most used models to describe the chemo-sorption of a substrate into a solid surface without product desorption. In this reaction, adsorption yield decreases with time due to the surface coverage increase. The Elovich model is generally described by the expression indicated in Eq. (8) [19]:

$$\frac{dq(t)}{dt} = \alpha \cdot \exp(-\beta \cdot q(t)) \quad (8)$$

The integration of Eq. (8) gives the form presented in Eq. (9):

$$q(t) = \frac{1}{\beta} \cdot \ln(\alpha \cdot \beta) + \frac{1}{\beta} \cdot \ln(t) \quad (9)$$

where: α is the initial adsorption rate ($\text{mg g}^{-1} \text{min}^{-1}$) and β is the desorption constant (g mg^{-1}).

2.5 Biosorption isotherm modeling

The need to design low-cost adsorbents to treat industrial effluents has been an interesting concern for most environmental researchers. So modeling of experimental data from adsorption processes is a very important means of predicting the mechanisms of various adsorption systems modeling [20].

Equilibrium adsorption isotherms of AO 51, RR 75 and DB 86 on the studied biomass were analyzed according to the most studied models: Langmuir, Freundlich, Temkin (two parameters models), Redlich–Peterson and Toth (three parameters models), since they are among the most used models in the literature and each of them presents a different

theory of adsorption mechanism. These models suggested not only whether the adsorption is single-layer or multi-layer, but also parameters involved in adsorption mechanism.

2.5.1 Langmuir model

Langmuir proposed an isotherm model for gases adsorbed into solids, which explains adsorption by considering that an adsorbent behaves as an ideal gas at isothermal conditions. Langmuir proposed his theory by making the following assumption [21]:

$$q_e = \frac{q_m \cdot K_L \cdot C_e}{1 + K_L \cdot C_e} \quad (10)$$

where: q_e is the equilibrium adsorbent concentrations in solution (mg g^{-1}); q_m is the maximum adsorption capacity of the adsorbent (mg g^{-1}); K_L is the Langmuir equilibrium constant (L mg^{-1}) and C_e is the equilibrium dye concentration (mg L^{-1}).

The validity of the Langmuir adsorption equation was tested by plotting the linear isotherm described by the following Eq. (11):

$$\frac{C_e}{q_m} = \frac{1}{q_m \cdot K_L} + \frac{C_e}{q_m} \quad (11)$$

2.5.2 Freundlich model

The Freundlich model is applied to describe adsorption on heterogeneous adsorbent surfaces and the interaction between adsorbed molecules [22]. Freundlich isotherm application suggests that the adsorption energy exponentially decreases. This isotherm is an empirical equation and can be employed to describe multilayer adsorption as shown in the following expression Eq. (12):

$$q_e = K_F \cdot C_e^{1/n} \quad (12)$$

where: K_F is the Freundlich constant describing the adsorbent adsorption capacity ($\text{mg}^{-1/n} \text{g}^{-1} \text{L}^{1/n}$) and n is the heterogeneity factor related to the adsorption intensity.

2.5.3 Temkin model

Temkin isotherm model considers the effect of some indirect adsorbate/adsorbate interactions and suggests that the heat of adsorption of all the molecules in the layer would linearly decrease with coverage [23]. It has been generally applied in the following form Eq. (13):

$$q_e = \frac{R \cdot T}{b} \ln(A \cdot C_e) \quad (13)$$

The equation can be linearized as:

$$q_e = B \cdot \ln(A) + B \cdot \ln(C_e) \quad (14)$$

where: $B = \frac{R \cdot T}{b}$ is the Temkin constant related to heat of adsorption (J mol^{-1}); A is the Temkin isotherm constant (L g^{-1}); R is the gas constant ($8.314 \text{ J mol}^{-1} \text{ K}$) and T is the absolute temperature (K).

2.5.4 Redlich–Peterson model

Redlich–Peterson isotherm [24] incorporated the features of the Langmuir and Freundlich isotherms into a single equation and presented a general isotherm equation as indicated in Eq. (15):

$$q_e = \frac{K_{RP} \cdot C_e}{1 + \alpha_{RP} \cdot C_e^{\beta_{RP}}} \quad (15)$$

where: K_{RP} is the Redlich–Peterson model isotherm constant (L g^{-1}); α_{RP} is the Redlich–Peterson model isotherm constant (L mg^{-1}) and β_{RP} is the Redlich–Peterson model exponent. The exponent β_{RP} lies between 0 and 1. There are two limiting behaviors: Langmuir for $\beta_{RP} = 1$ and Henry's law from for $\beta_{RP} = 0$.

2.5.5 Toth model

The Toth isotherm model, derived from the potential theory, was proven to be useful in describing the adsorption of heterogeneous systems, such as phenolic compounds on carbon [25]. It assumes an asymmetrical quasi-Gaussian energy distribution with a widened left-hand side, so most sites have adsorption energy lower than the mean value. It can be represented as:

$$q_e = \frac{q_m \cdot b_T \cdot C_e}{[1 + (b_T \cdot C_e)^{n_T}]^{1/n_T}} \quad (16)$$

where: q_m is the maximum adsorption capacity of the adsorbent (mg g^{-1}); b_T is the Toth model constant and n_T is the Toth model exponent.

It is obvious that for $n_T = 1$, the isotherm reduces to the Langmuir adsorption isotherm equation.

2.6 Statistical analysis

All fitting tests were established using a Matlab 2010 algorithm involving the nonlinear least-square regression method. The fitting quality was tested using the four usual statistical criteria which are: coefficient of determination (R^2), adjusted coefficient of determination (R^2_{Adj}), root mean square error (RMSE) and sum of square errors (SSE). Model presenting the best fitting is characterized by high R^2 and R^2_{Adj} ($\sim 100\%$) and low RMSE and SSE (~ 0). All

model coefficients were determined with 95% confidence level (corresponding $\text{top} < 0.05$).

2.7 Biosorbent characterization

The average size of bio-sorbent particles was measured by the mean of the Laser Particle Sizer (LPS) ANALYSETTE 22 NanoTec.

In order to identify the functional groups responsible for the adsorption phenomena, FT-IR spectroscopy analyses of the bio-sorbent materials before and after dye removal were performed. FT-IR spectra, within the range of $650\text{--}4000 \text{ cm}^{-1}$ of bio-sorbent, were recorded using a Cory 630 FT-IR, Agilent technologies spectrophotometer.

SEM micrographs were taken to investigate textural changes on the bio-sorbent surface before and after dye adsorption. Analysis were conducted by a scanning electron microscope JEOL (JFC-1100 E) using an accelerating voltage of 15 kV.

3 Results and discussion

3.1 Effect of initial pH on dye removal efficiency

Previous studies on dye bio-sorption by heat-treated fungal biomass have shown that initial pH has a significant effect on dye adsorption capacity of the fungus [26, 27]. In this study, the effect of pH on dye removal was studied at pH values ranging from 2 to 12 for each fungal biomass-dye system. For each pH value, experimental conditions were kept constant: dye concentration (50 mg L^{-1}), bio-sorbent quantity (1 g L^{-1}), temperature ($30 \text{ }^\circ\text{C}$) and shaking speed (150 rpm). In Fig. 1 is shown that for AO51, the dye removal rate decreased from 92 to 42% by increasing the pH from 2.0 to 12.0. On the other hand, the removal of the dyes RR75 and DB86 declined sharply above pH 2.0 from 95 to 4% and from 98 to 2%, respectively.

The pH of the medium affects not only the surface charge of the biomass and the solubility of dye, but also the adsorption mechanism. The surface of the fungal biomass is generally charged at different pH values due to the presence of ionized groups such as carboxyl, phosphate and amino, so an electrostatic attraction could be created between the biomass charged positively and the anionic dyes charged negatively [28–31]. At alkaline pH conditions, adsorption decreased due to the competition between the dye anions and the hydroxyl anions for the positively-charged binding sites [32]. However, low pH has been found to enhance anionic dyes uptake by the biomass of yeast and fungi [33] and also by other adsorbent materials such as almond shells used to remove the anionic dye Direct Red 80 [34] and beech wood sawdust used to remove anionic direct dyes [35]. Since the

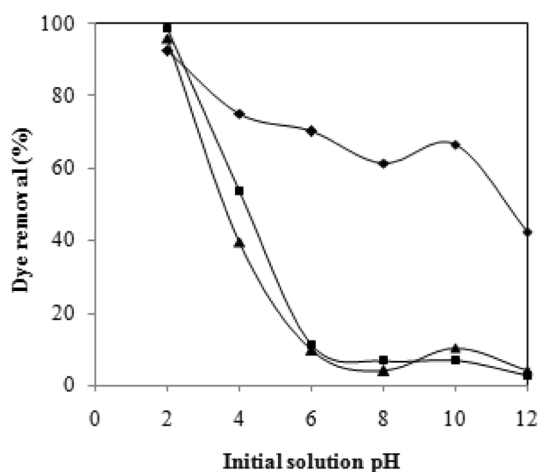


Fig. 1 Effect of pH on dye removal efficiency by heat-treated biomass (bio-sorbent quantity = 1.0 g L^{-1} , dye concentration = 50 mg L^{-1} , contact time = 60 min, temperature = $30 \text{ }^\circ\text{C}$, shaking rate = 150 rpm). “Diamond”: AO 51; “Triangle”: RR 75; “Square”: DB 86

maximum removal of the three dyes occurred at pH 2.0 after 1 h of contact time, all further studies were carried out at this pH value.

3.2 Effect of contact time

In order to examine the kinetics of dye binding capacity, the three dyes were incubated with the bio-sorbent for 120 min at different pH values. Samples were withdrawn each 30 min and analyzed for residual dye concentration. Results presented in Fig. 2 show that the rate of dye uptake was very quick at the beginning, with a maximum removal in the first 30 min of over 80%, 81% and 96% for AO 51, RR 75 and DB 86, respectively. After this initial fast phase, the adsorption rate slowed down and reached a plateau after 60 min, which indicates the equilibrium state of the system. An important quantity of all three dyes was removed within the first 10 min of the beginning of the interaction. Then, the uptake rate gradually decreased until reaching the equilibrium at about 60 min after which no appreciable increase in the removal efficiency was detected.

This rapid rate of dye removal by fungal biomass has significant practical importance for applications in reactors of small volume, so ensuring efficiency and economy [10]. During the first phase of adsorption, the fast uptake of the dyes might be due to high availability of adsorption sites on the bio-sorbent. After that, the significant decline in the adsorption capacity was caused by the reduction in the available adsorption sites in addition to the repulsive forces between the dyes molecules on the biomass and the bulk phase [36].

On the other hand, the variation in molecular structure and ionic radius between dye molecules has been considered

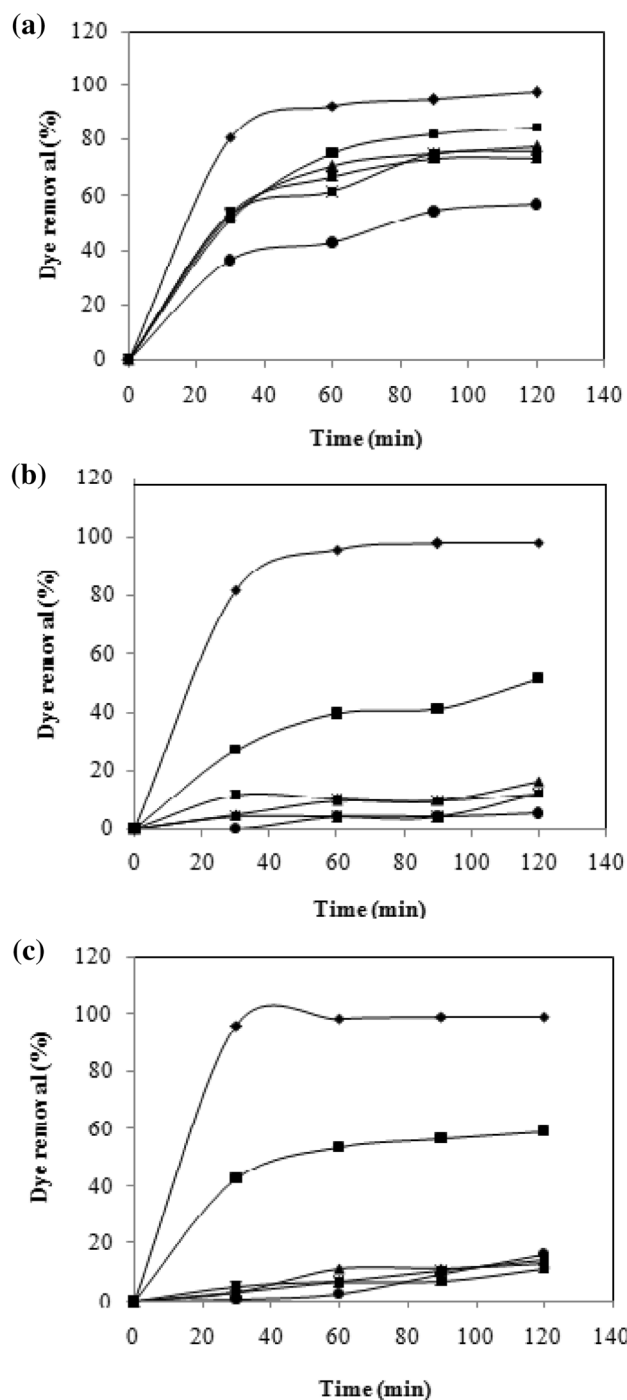


Fig. 2 Kinetics of dye removal by heat-treated biomass at different pH values (bio-sorbent quantity = 1 g L^{-1} , dye concentration = 50 mg L^{-1} , temperature = $30 \text{ }^\circ\text{C}$, shaking rate = 150 rpm) for AO 51 (a), RR 75 (b) and DB 86 (c). “Diamond”: pH 2; “Square”: pH 4; “Triangle”: pH 6; “Times”: pH 8; “Asterisk”: pH 10; “Circle”: pH 12

as the main reason for different bio-sorption of dyes onto fungal and algal biomasses [26, 37].

3.3 Effect of bio-sorbent dosage

The relationship between the amount of bio-sorbent and dye adsorption was investigated for six different biomass concentrations, ranging from 0.25 to 1.25 mg L⁻¹. Increasing biomass loading from 0.25 to 1 g L⁻¹ increased the removal percentage for the three dyes (Fig. 3).

There was no significant difference in dye adsorption when the bio-sorbent dosage was higher than 1 g L⁻¹. Therefore, the optimum biomass dosage for a maximum dye bio-sorption was 1 g L⁻¹ for each dye for a contact time of 60 min. Thus, maximum dye removal efficiencies were 94.9, 97.3 and 99.6% for AO 51, RR 75 and DB 86, respectively. This fact could be explained by the higher the amount of bio-sorbent used, the higher the number of available adsorption sites, there by the higher the adsorbed dye molecules.

3.4 Effect of initial dye concentration

In this study, the effect of initial dye concentration on dye removal was studied at different concentrations ranging from 12.5 to 1000 mg L⁻¹ at 30 °C, 1 g L⁻¹ biomass dosage and pH 2.0. As shown in Fig. 4, color removal by the biomass was high for all dyes at initial dye concentrations between 12.5 and 50 mg L⁻¹ (>98% for AO 51, >97% for RR 75 and >99% for DB 86) and sharply decreased from 100 mg L⁻¹ onwards.

Mohan et al. [38] reported that the initial dye concentration provides an important driving force to overcome the diffusive mass transfer resistance of all molecules between the adsorbate and the adsorbent. Moreover, the adsorption process is enhanced by the increasing of the number of collisions between the dye anions and the bio-sorbent. However, the adsorption yield decreased significantly at higher dyes concentrations (> 100 mg L⁻¹). This can be explained by the saturation of the available binding sites on the bio-sorbent [39].

3.5 Effect of temperature on dye removal by fungal biomass

The effect of temperature on dye removal by *Neonectria radiculicola* dead biomass was investigated for different temperature values (30–60 °C) under static conditions at pH=2.0 and a contact time of 60 min. As illustrated in Fig. 5, the removal percentage increased slightly from 91 to 95% for AO 51 and from 92 to 97% for RR 75, on the contrary for DB 86 the removal percentage decreased slightly from 99.9 to 98.6%, when the temperature increased from 30 to 60 °C.

The removal efficiency of the three dyes at different studied temperatures showed that the bio-sorption is independent on this factor. This result makes this bio-sorbent suitable for

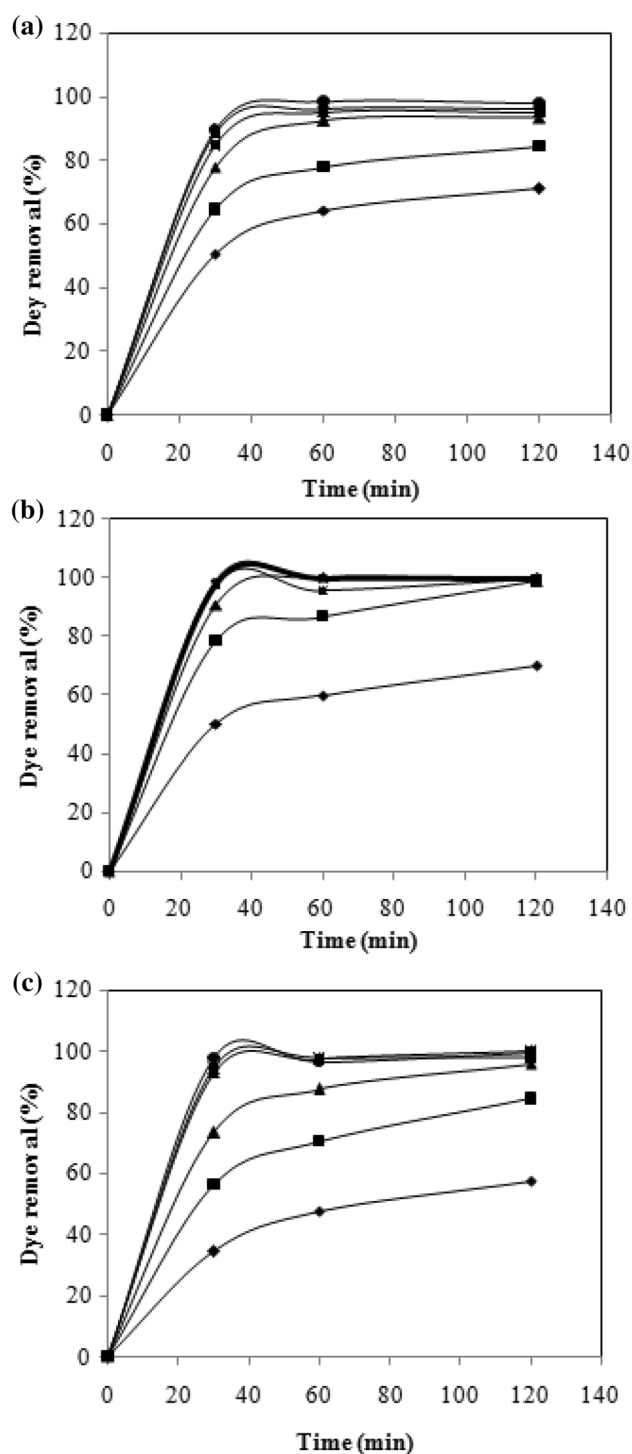


Fig. 3 Effect of bio-sorbent dosage on dye removal efficiency (dye concentration = 50 mg L⁻¹, pH = 2.0, temperature = 30 °C, shaking rate = 150 rpm) for AO 51 (a), RR 75 (b) and DB 86 (c). “Diamond”: 0.25; “Square”: 0.5; “Triangle”: 0.75; “Times”: 1.0; “Asterisk”: 1.25; “Square”: 1.5 g L⁻¹

use at industrial-scale for treatment of dye wastewater via bio-adsorption technology.

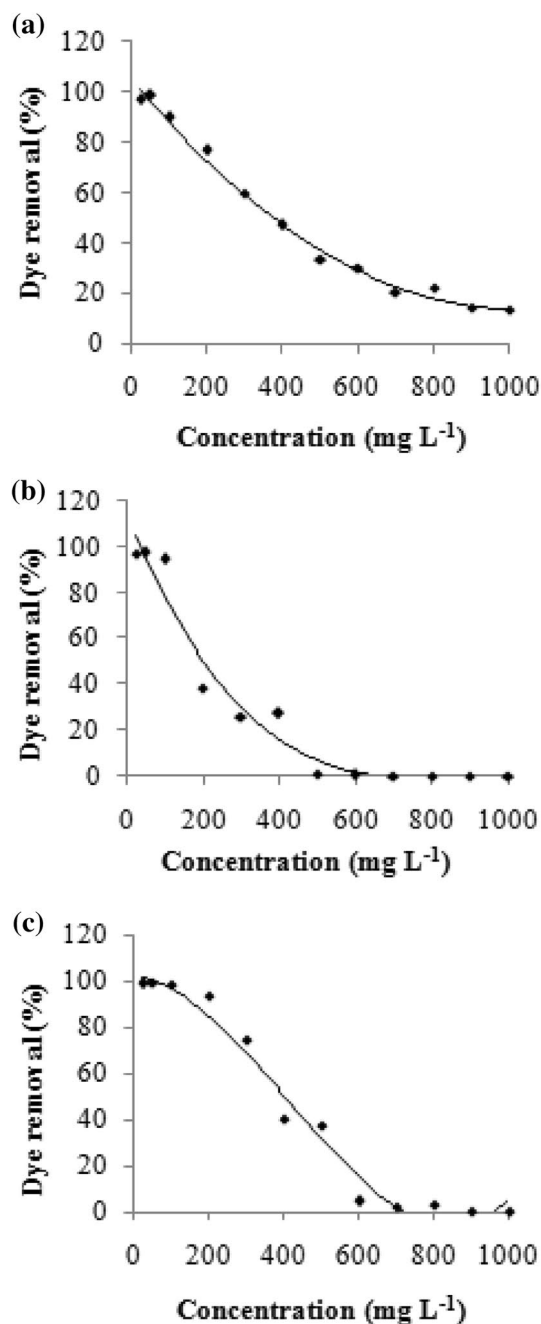


Fig. 4 Effect of initial dye concentration on dye removal efficiency (bio-sorbent quantity = 1 g L⁻¹, pH = 2.0, temperature = 30 °C, shaking rate = 150 rpm) for AO 51 (a), RR 75 (b) and DB 86 (c)

3.6 Bio-sorption kinetics modeling

To compute the bio-sorption capacity of the bio-sorbent at equilibrium, samples were collected at various times (10–60 min). The kinetics results for the three defined dyes and for initial concentrations of 50 and 100 mg L⁻¹ are given in Tables 2 and 3, respectively. Also, the statistical (R^2 , R^2_{adj} , RMSE and SEE) and models parameters are presented in

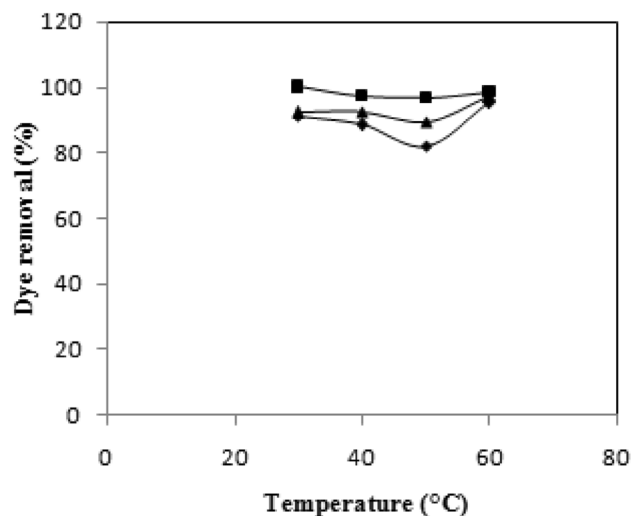


Fig. 5 Effect of temperature on dye removal efficiency by heat-treated biomass (bio-sorbent quantity = 1.0 g L⁻¹, dye concentration = 50 mg L⁻¹, contact time = 60 min, pH = 2.0, shaking rate = 150 rpm). “Diamond”: AO 51; “Square”: RR 75; “Triangle”: DB 86

Tables 2 and 3 in order to compare the different fitting quality of models.

As it can be shown, both the pseudo-first and pseudo-second order models fitted well the experimental data, with R^2 and $R^2_{adj} \geq 0.998$. In Fig. 6a, b, the comparison between the experimental data and the calculated ones by the pseudo-first order model, with the identified parameters for the two initial concentrations of 50 and 100 mg g⁻¹, is shown. Moreover, the bio-sorption capacities (q_e) estimated by the models were also very close to those obtained by the experiments (~50 mg L⁻¹).

In fact, most of the bio-sorption studies reported the pseudo-second order model is widely adopted to describe such as mechanism while it gives a reasonably good fit of data, over the entire fractional approach to equilibrium [36]. In contrast, the intra-particle diffusion and Elovich models, all the determination and adjusted determination coefficients found were lower than 0.78. From all results, it could be presumed that dye adsorption by all biomass systems were controlled by chemo-sorption in which the valence forces, as covalent bonds and/or ion exchange, between the adsorbent and the adsorbate exist until the surface active sites were occupied. Then, the dyes molecules were diffused into the bio-sorbent for other interactions [36]. The applicability of the intra-particle diffusion model suggested that the adsorption process of dyes was a complex mechanism in which boundary layer and intra-particle diffusion co-exist. However, dye diffusion within the biomass seemed to be much slower than dye transfer from the bulk solution to the outer biomass surface [40, 41].

Table 2 Kinetic models parameters for the bio-sorption of the dyes Acid Orange 51, Reactive Red 75 and Direct Blue 86 on *N. radicularis* biomass at an initial dye concentration of 50 mg L⁻¹

Models parameters	Dyes		
	AO 51	RR 75	DB 86
Pseudo-first order			
q_e (mg L ⁻¹)	47.629	48.927	49.791
k_1 (min ⁻¹)	0.074	0.099	0.127
R ²	1	1	1
R ² _{adj}	1	1	1
RMSE	0.261	0.090	0.012
SSE	0.204	0.024	0.0004
Pseudo-second order			
q_e (mg L ⁻¹)	49.364	49.823	50.165
k_2 (g mg ⁻¹ min)	0.005	0.010	0.024
R ²	0.998	1	1
R ² _{adj}	0.998	1	1
RMSE	1.020	0.342	0.201
SSE	3.122	0.351	0.121
Intraparticle diffusion model			
K_p (mg g ⁻¹ min ^{-1/2})	3.424	3.479	3.509
c (mg L ⁻¹)	11.202	12.455	13.229
R ²	0.729	0.695	0.674
R ² _{adj}	0.639	0.594	0.565
RMSE	12.490	13.770	14.610
SSE	467.6	569.1	640.7
Elovich model			
α (mg g ⁻¹ min ⁻¹)	234.814	4570	9.358·10 ⁴
β (g mg ⁻¹)	0.100	0.168	0.231
R ²	0.712	0.818	0.342
R ² _{adj}	0.712	0.727	0.012
RMSE	1.377	0.642	0.540
SSE	5.691	0.824	0.584

Table 3 Kinetic models parameters for the bio-sorption of the dyes Acid Orange 51, Reactive Red 75 and Direct Blue 86 on *N. radicularis* biomass at an initial dye concentration of 100 mg L⁻¹

Models parameters	Dyes		
	AO 51	RR 75	DB 86
Pseudo-first order			
q_e (mg L ⁻¹)	97.378	97.359	99.516
k_1 (min ⁻¹)	0.202	0.132	0.256
R ²	1	0.998	1
R ² _{adj}	1	0.998	1
RMSE	0.634	1.400	0.525
SSE	2.412	11.760	1.656
Pseudo-second order			
q_e (mg L ⁻¹)	102.675	108.288	102.705
k_2 (g mg ⁻¹ min)	0.005	0.002	0.010
R ²	0.999	0.999	1
R ² _{adj}	0.999	0.998	1
RMSE	1.207	1.350	0.807
SSE	8.739	10.930	3.905
Intraparticle diffusion model			
k_p (mg g ⁻¹ min ^{-1/2})	12.287	12.815	12.321
c (mg L ⁻¹)	27.316	20.931	30.219
R ²	0.713	0.813	0.674
R ² _{adj}	0.665	0.782	0.619
RMSE	19.51	15.36	21.440
SSE	2283	1415	2757
Elovich model			
α (mg g ⁻¹ min ⁻¹)	4.035 × 10 ⁴	2.552 × 10 ⁴	5.720 × 10 ⁴
β (g mg ⁻¹)	0.100	0.100	0.100
R ²	0.592	0.367	0.770
R ² _{adj}	0.592	0.367	0.770
RMSE	2.977	7.246	1.350
SSE	53.17	315.1	10.930

3.7 Bio-sorption isotherm modeling

To design the adsorption system, the investigation of the equilibrium bio-sorption is very important in order to determine the capacity of the bio-sorbent. In the present study, the previously presented five isotherm models were applied to the equilibrium adsorption data of AO 51, RR 75 and DB 86 dyes on *N. radicularis* heat-treated biomass. As 400 mg L⁻¹ was the concentration of saturation for fungal biomass, the evaluation of bio-sorption kinetics and isotherms was studied for concentrations ranging from 12.5 to 400 mg L⁻¹. In Table 4, the values of the identified isotherm model parameters and their correlation coefficients are presented.

The modeling of adsorption experimental data of the three dyes led to good values of correlation coefficients for almost all the studied models. Results show that for AO 51 and DB 86, all models gave a high R² > 0.94, and for

RR 75, only the Freundlich and Temkin models have a low R² (~0.70). In fact, the Readlich–Peterson model was the best one to describe the adsorption mechanism for all dyes, according to the comparison of the statistical parameters with maximum adsorption capacities of 120.6, 75.37 and 200.5 L g⁻¹ for AO 51, RR 75 and DB 86, respectively. Dyes' β_{RP} values are less than 1 (except for RR 75). In fact, large molecule adsorption, as the case of dyes, is not easy in accordance with the theory of monolayer adsorption upon which the Langmuir isotherm equation is based. This is because impediments exist between pores and adsorbate, so the β_{RP} value is usually less than 1 [42]. In Fig. 7, the graphical results obtained by the Readlich–Peterson model are shown.

The calculated results fitted well the experimental data for the three dyes. Moreover, values of R² and R²_{adj} obtained by the Freundlich model were higher than those obtained by the

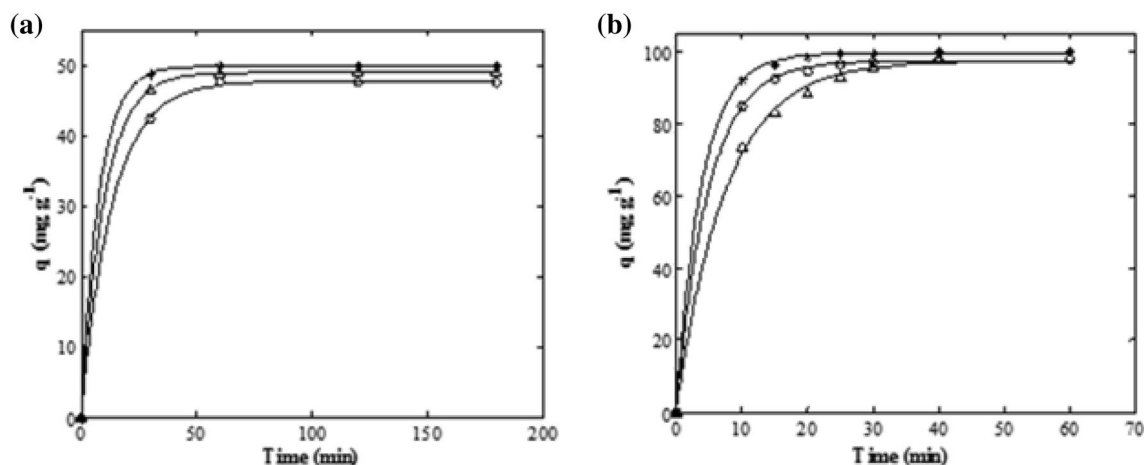


Fig. 6 Modeling results of adsorption kinetics experimental data of the three dyes with initial concentrations of 50 mg L⁻¹ (a) and 100 mg L⁻¹ (b). “Open circle”: AO 51; “Open triangle”: RR 75; “Asterisks”: DB 86 and “Dash”: Pseudo-first order model

Langmuir one in almost all cases, indicating the acceptability of the model of heterogeneous adsorption mechanism for the fungal-dye system. Results showed that the removal efficiency of three dyes by the same biosorbent is different from each other (RR 75 < AO 51 < DB86). The important value of Freundlich constant ($KF = 71.18 \text{ mg}^{-1/n} \text{ g}^{-1} \text{ L}^{1/n}$) for DB 86, can be explained by the high capacity of the fungal biomass to uptake this dye rather than the other two dyes due to structural differences [36]. In fact, DB 86 ($780.16 \text{ g mol}^{-1}$), which is a phthalocyanine dye, owns two negative charges, four benzene rings in a non-linear structure, an atom of Cu in the center and has the lowest molecular weight. However, AO 51 ($860.795 \text{ g mol}^{-1}$) and RR 75 ($990.779 \text{ g mol}^{-1}$), which are azo dyes, has six benzene rings in a fairly linear structure with three and four negative charges, respectively. It likes that due to negative charges, linear structure 463 to line, high molecular weight and lot of side chains, dye molecules are less attractable by heat treated biomass of *Neonectria radicularis* [22].

Many studied shows a great potential to remove dyes by native, treated or modified fungal biomass. Depending on the nature of the interaction between biomass and dyes molecules, different isotherms were applicable and describe more the equilibrium of biomass-dye system. The native and treated fungal biomass of *Phanerochaete chrysosporium* was used for the biosorption of a textile dye (i.e., Reactive Blue 4). The dye uptake capacities of the biosorbents at 600 mg L^{-1} dye concentration were found to be 132.5, 156.9, 147.6 and 81.1 mg g^{-1} for native and heat-, acid- and base-treated dry fungal preparations, respectively. The dye uptake capacity order of the fungal preparations was found as heat-treated > acid-treated > native > base-treated. The Freundlich and Temkin models were able to describe the biosorption equilibrium of Reactive Blue 4 on native and

treated fungal preparations [43]. A previous study reported that the biosorption capacities of the native and heat-treated fungal biomass were found to be 101.1 and 152.3 mg g^{-1} for DB-1 and these were 189.7 and $225.4 \text{ mg dye/g biomass}$ for DR-128, respectively. The Freundlich and Temkin models were able to describe the biosorption equilibrium of DB-1 and DR-128 on the native and heat-treated fungal. The Freundlich model also showed that the small molecular weight dye (i.e., DR-128) had a higher affinity of adsorption than of the higher molecular weight dye (i.e., DB-1). Others studies focused on using cetyl trimethyl ammonium bromide (CTAB) modified *Aspergillus versicolor* biomass (AVB) as biosorbent to remove reactive black 5 (RB5). Biosorption isotherm data followed Langmuir isotherm model and the maximum biosorption capacity was 227.27 mg g^{-1} [44]. *Aspergillus niger* biomass also show a high capacity uptake of the textile dye Acid yellow 99 with a maximum adsorption capacity of 544.30 mg g^{-1} . The isotherm data can best be explained by Redlich–Peterson model suggesting a possible physical and chemical adsorption of the dye molecules on the surface of the biomass [45]. Industrial microbial waste of *Aspergillus niger* was utilized as novel adsorbent to remove two cationic dyes (crystal violet, CV; methylene blue, MB). The Langmuir model provided a good fit of the experimental data with the maximum monolayer adsorption (q_m) of 175.4 mg g^{-1} and 92.6 mg g^{-1} for CVs and MBs, respectively in the single dye system [46].

Table 4 Modeling results of the bio-sorption isotherms of the dyes Acid Orange 51, Reactive Red 75 and Direct Blue 86 on *N. radicola* biomass (T = 30 °C)

Models parameters	Dyes		
	AO 51	RR 75	DB 86
Langmuir			
q_m (mg g ⁻¹)	199.158	112.823	227.1
K_L (mg g ⁻¹)	0.113	0.880	0.402
R ²	0.952	0.865	0.943
R ² _{adj}	0.946	0.849	0.936
RMSE	16.520	15.310	22.52
SSE	2456	2111	4566
Freundlich			
K_F (mg ^{-1/n} g ⁻¹ L ^{1/n})	48.636	53.783	71.180
N	3.538	6.952	3.790
R ²	0.981	0.664	0.956
R ² _{adj}	0.979	0.626	0.951
RMSE	10.39	24.130	19.69
SSE	971.2	5242	3488
Temkin			
A (L g ⁻¹)	7.842	55.260	9.310
B	95.864	201.2	73.898
R ²	0.950	0.730	0.984
R ² _{adj}	0.944	0.700	0.982
RMSE	16.860	21.63	12.060
SSE	2558	4210	1309
Redlich–Peterson			
K_{RP} (L g ⁻¹)	120.6	83.606	200.5
α_{RP} (L mg ⁻¹)	1.836	0.584	1.767
β_{RP}	0.778	1.050	0.839
R ²	0.991	0.876	0.984
R ² _{adj}	0.988	0.846	0.980
RMSE	7.754	15.510	12.51
SSE	481	1925	1252
Toth			
q_m (mg g ⁻¹)	532.1	108.5	680.8
b_T	3.370	0.561	1.349
n_T	0.223	30.796	0.330
R ²	0.991	0.890	0.980
R ² _{adj}	0.989	0.863	0.975
RMSE	7.485	14.610	14.19
SSE	448.2	1708	1610

3.8 FT-IR and SEM analyses of the bio-sorbent before and after adsorption of dyes

3.8.1 FT-IR analyses

FTIR spectra in the range of 4000–600 cm⁻¹ of fungal biomass before dye adsorption were conducted to identify

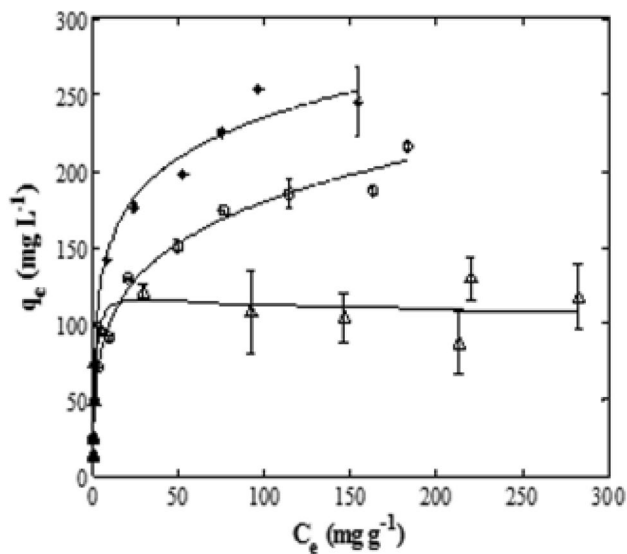


Fig. 7 Modeling results of adsorption isotherm experimental data of the three dyes. “Open circle”: AO 51; “Open triangle”: RR 75; “Asterisks”: DB 86 and “Dash”: Redlich–Peterson model

potential functional groups that may be responsible for the dyes binding (Fig. 8 spectrum a).

The band at 3262 cm⁻¹ corresponded to the stretching vibration of bonded and non-bonded hydroxyl groups and water. Peaks at 2921 and 2854 cm⁻¹ indicated the presence of both symmetrical and asymmetrical C-H stretching, corresponding to aliphatic methylene groups. The sharp peak at 1630 cm⁻¹ is attributed to the stretching vibration of the C=C, C=O and COO⁻ groups of cyclic alkenes, ketones, aldehydes and carboxylic acids. The peak at 1533 cm⁻¹ can be explained by the presence of amide I and amide II stretching, corresponding to the cell proteins. The band at 1416 cm⁻¹ describes the CH₂ binding of lipids. The peak observed at 1319 cm⁻¹ reflects the vibration of C–O groups

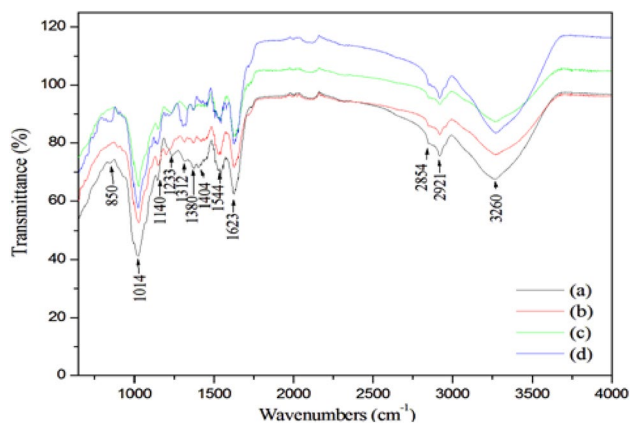


Fig. 8 FT-IR spectra of biomass before (a) and after adsorption of RR 75 (b), DB 86 (c) and AO 51 (d)

from carboxylate ions. Nucleic acid and phospholipids are described by the asymmetric stretching of PO^{2-} groups at 1233 cm^{-1} . The peak at 1020 cm^{-1} is due to the stretching vibration of C–O–C, C–O, C–O–H, C–O–P groups of esters, phosphodiester and polysaccharides. Therefore, the heat-treated biomass of *N. radicularis* revealed the presence of all the typical peaks corresponding to the main biochemical cell components (i.e. lipids, proteins, nucleic acids and carbohydrates) with a variety of functional groups such as carboxyl, hydroxyl, aldehydes, ketones amide, and phosphate on its surface which may improve dye uptake by the biomaterial.

The FTIR spectra of biomass after dye adsorption presented some shifts in the in the range of $3200\text{--}2800\text{ cm}^{-1}$ suggesting the involvement of both carboxyl and hydroxyl groups in the AO 51, RR 75 and DB 86 uptake (Fig. 8, spectra b, c and d). Spectra in the range of the $1600\text{--}1000\text{ cm}^{-1}$ presented significant changes in peak intensity and wave values in the dyes-loaded biomass compared to the initially used biomaterial. Peaks interestingly shifted after AO 51, RR 75 and DB 86 uptake, suggesting an interaction of dyes molecules with the previously described functional groups in this region. New peaks were identified at 1505 and 1199 cm^{-1} respectively in AO 51 and RR 75 spectra after adsorption, while peak at 1416 cm^{-1} disappeared in the AO 51 containing biomass. The shift of various adsorption bands to a higher or lower frequency after dye adsorption confirmed that these functional groups were responsible for the uptake of the three dyes. After AO 51 adsorption, a peak at 1505 cm^{-1} appeared which was attributed to aromatic ring vibration while the peaks appeared at 1199 cm^{-1} after RR 75 adsorption, were attributed to C–O formation. Figure 9 illustrates the mechanism of interaction between the bio-sorbent and AO 51, RR 75 and DB86.

3.8.2 SEM analyses

Morphological analyses of the used adsorbent before and after dye adsorption were conducted to illustrate morphological changes on the surface resulting by dyes binding (Fig. 9).

Morphological analysis of *N. radicularis* heat-treated biomass before dye adsorption showed that the biomaterial was an agglomerate of filamentous particles with irregular and broken edges. The presence of cavities and differences in the particle shape and size conferred the bio-sorbent its ability to accumulate adsorbate molecules (Fig. 10a). After biosorption, the three used dyes clearly affected the surface morphology of the biomass. Dye molecules were trapped into the particle pores and masked the edged relief characterizing the bio-sorbent surface. The adsorbed dyes decreased the whole surface porosity and roughness the initial material (Fig. 10a–d).

4 Conclusion

The present study revealed that the bio-sorbent material prepared from the biomass of *Neonectria radicularis* could be used to remove efficiently three textile dyes (AO 51, RR 75 and DB 86) from aqueous solutions. pH of the solution, bio-sorbent dosage, contact time and initial dye concentration affected the bio-sorption capacity of the biomass. The bio-sorption capacity of the three dyes onto fungal biomass increased in the following order $\text{DB 86} > \text{AO 51} > \text{RR 75}$ because of the difference in the size and the chemical structure of the different dyes. The kinetics studies of the three dyes were fitted well by the pseudo-first order rate equation and the bio-sorption equilibrium isotherms were well described by the Redlich–Peterson model.

Fig. 9 Mechanism of interaction between the bio-sorbent and AO 51, RR 75 and DB86

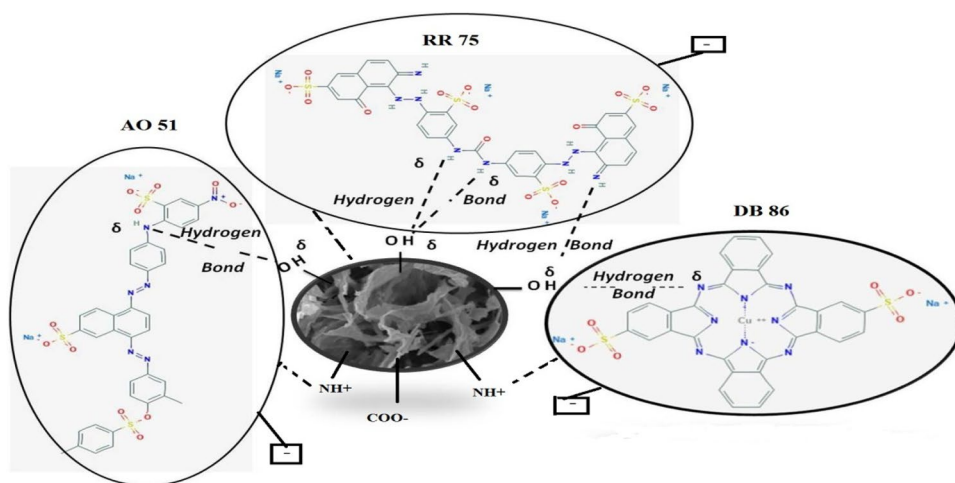
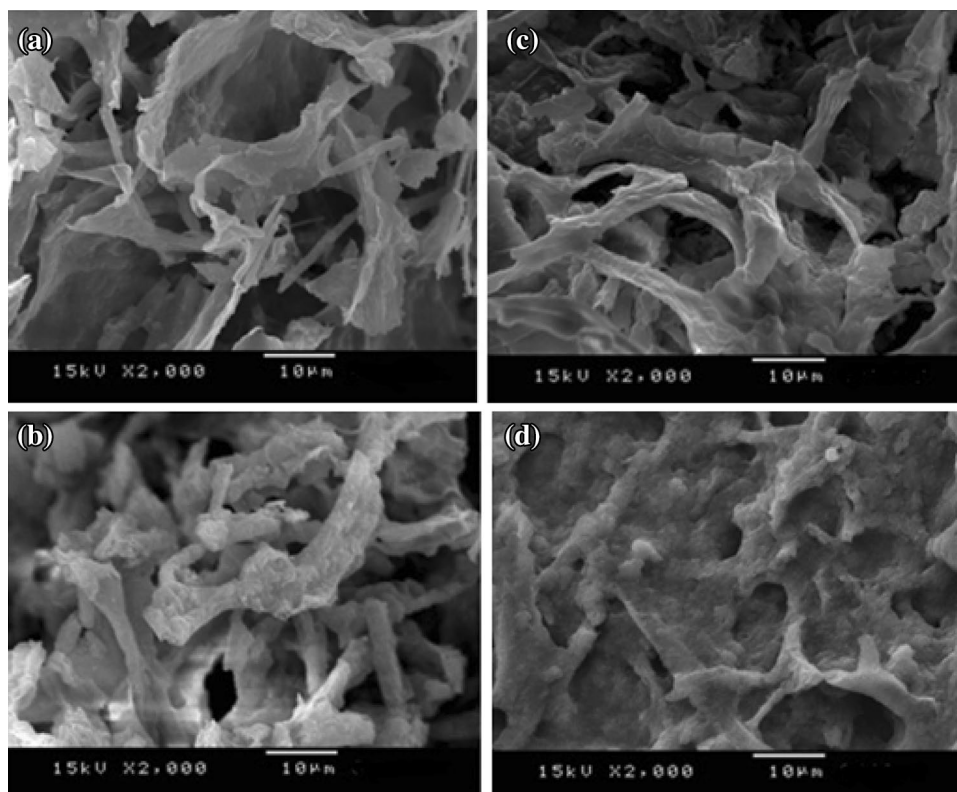


Fig. 10 SEM images of biomass before (a) and after adsorption of AO 51 (b), RR 75 (c) and DB 86 (d)



Acknowledgements This work was supported by the Ministry of Higher Education and Scientific Research of Tunisia. The authors gratefully acknowledge the Materials Engineering Department of the National School of Engineering of Sfax for its help in performing the FTIR spectroscopy analyses. This research did not receive any specific grant from funding agencies in the public, commercial, or not-for-profit sectors.

Compliance with ethical standards

Conflict of interest The authors declare that they have no conflict of interest.

References

- M.T. Yagub, T.K. Sen, H.M. Ang, *Water Air Soil Pollut.* **223**, 5267 (2012)
- N. Mathur, P. Bhatnagar, *J. Environ. Biol.* **28**, 123 (2007)
- I. Louati, M. Fersi, B. Hadrich, B. Ghariani, M. Nasri, T. Mechichi, *3 Biotech* **8**, 478 (2018)
- R.F. Gomes, A.C.N. de Azevedo, A.G.B. Pereira, E.C. Muniz, A.R. Fajardo, F.H.A. Rodrigues, *J. Colloid Interface Sci.* **454**, 200 (2015)
- G. Crini, *Bioresour. Technol.* **97**, 1061 (2006)
- F.I. Hai, K. Yamamoto, K. Fukushi, *Crit. Rev. Environ. Sci. Technol.* **37**, 315 (2007)
- T. Robinson, G. McMullan, R. Marchant, P. Nigam, *Bioresour. Technol.* **77**, 247 (2001)
- G. Olivieri, A.D. Donato, A. Marzocchella, P. Salatino, *Biodegrad Azo Dyes* (Springer, Berlin, 2010), pp. 101–131
- W. Li, B. Mu, Y. Yang, *Bioresour. Technol.* (2019)
- Z. Aksu, *Process Biochem.* **40**, 997 (2005)
- B. Mu, A. Wang, *J. Environ. Chem. Eng.* **4**, 1274 (2016)
- G.M. Gadd, *J. Chem. Technol. Biotechnol.* **84**, 13 (2009)
- O. Yesilada, D. Asma, S. Cing, *Process Biochem.* **38**, 933 (2003)
- G. Bayramoğlu, I. Tuzun, G. Celik, M. Yilmaz, M.Y. Arica, *Int. J. Miner. Process.* **81**, 35 (2006)
- D. Daâssi, H. Zouari-Mechichi, L. Belbahri, J. Barriuso, M.J. Martínez, M. Nasri, T. Mechichi, *3 Biotech* **6**, 46 (2016)
- S. Lagergren, *K.vet.akad.handl.* **24**, 1 (1898)
- Y.S. Ho, G. McKay, *Process Biochem.* **34**, 451 (1999)
- W.J. Weber, J.C. Morris, *J. Sanit. Eng. Div.* **89**, 31 (1963)
- R.-S. Juang, M.-L. Chen, *Ind. Eng. Chem. Res.* **36**, 813 (1997)
- N. Ayawei, A.N. Ebelegi, D. Wankasi, *J. Chem.* (2017)
- I. Langmuir, *J. Am. Chem. Soc.* **40**, 1361 (1918)
- H.M.F. Freundlich, *J. Phys. Chem.* **57**, 385 (1906)
- M.I. Tempkin, V. Pyzhev, *Acta Physiochim.* **12**, 217 (1940)
- O. Redlich, D.L. Peterson, *J. Phys. Chem.* **63**, 1024 (1959)
- J. Toth, *Acta Chem. Acad. Hung.* **69**, 311 (1971)
- N.S. Maurya, A.K. Mittal, P. Cornel, E. Rother, *Bioresour. Technol.* **97**, 512 (2006)
- K. Kumari, T.E. Abraham, *Bioresour. Technol.* **98**, 1704 (2007)
- J. Wu, H.-Q. Yu, *J. Hazard. Mater.* **137**, 498 (2006)
- N. Barka, K. Ouzauit, M. Abdennouri, M.E. Makhfouk, *J. Taiwan Inst. Chem. Eng.* **44**, 52 (2013)
- M. El Haddad, R. Slimani, R. Mamouni, S. ElAntri, S. Lazar, *J. Assoc. Arab Univ. Basic Appl. Sci.* **14**, 51 (2013)
- M.V. Subbaiah, D.-S. Kim, *Ecotoxicol. Environ. Saf.* **128**, 109 (2016)
- Y. Safa, H.N. Bhatti, *Chem. Eng. Res. Des.* **89**, 2566 (2011)
- Z. Aksu, G. Dönmez, *Chemosphere* **50**, 1075 (2003)
- F. Doulati Ardejani, K. Badii, N.Y. Limaee, S.Z. Shafaei, A.R. Mirhabibi, *J. Hazard. Mater.* **151**, 730 (2008)

35. V. Dulman, S.M. Cucu-Man, *J. Hazard. Mater.* **162**, 1457 (2009)
36. A.R. Khataee, F. Vafaei, M. Jannatkhah, *Int. Biodeterior. Biodegrad.* **83**, 33 (2013)
37. A.R. Khataee, G. Dehghan, *J. Taiwan Inst. Chem. Eng.* **42**, 26 (2011)
38. S.V. Mohan, S.V. Ramanaiah, P.N. Sarma, *Biochem. Eng. J.* **38**, 61 (2008)
39. T. Murugan, A. Ganapathi, R. Valliappan, *J. Chem.* (2010)
40. M. Kousha, E. Daneshvar, M.S. Sohrabi, M. Jokar, A. Bhatnagar, *Chem. Eng. J.* **192**, 67 (2012)
41. M. Kousha, E. Daneshvar, M.S. Sohrabi, N. Koutahzadeh, A.R. Khataee, *Int. Biodeterior. Biodegrad.* **67**, 56 (2012)
42. F.-C. Wu, B.-L. Liu, K.-T. Wu, R.-L. Tseng, *Chem. Eng. J.* **162**, 21 (2010)
43. *J. Hazard. Mater.* **137**, 1689 (2006)
44. J. Huang, D. Liu, J. Lu, H. Wang, X. Wei, J. Liu, *Colloids Surf. Physicochem. Eng. Asp.* **492**, 242 (2016)
45. A. Naskar, R. Majumder, *J. Mol. Liq.* **242**, 892 (2017)
46. J. Liu, F. Chen, C. Li, L. Lu, C. Hu, Y. Wei, P. Raymer, Q. Huang, *J. Clean. Prod.* **208**, 552 (2019)

Publisher's Note Springer Nature remains neutral with regard to jurisdictional claims in published maps and institutional affiliations.